Derivation of Conductivity from Coordinated E- and F-Region ISR Measurements

1. INTRODUCTION

For several years the Sondrestrom ISR has probed the auroral ionosphere with a dual transmitter mode that simultaneously measures plasma parameters in the E region and F region [*Kelly et al.*, 1995]. The E-region mode, a 320 μs coded pulse, is modulated with a 20 μs subpulse to provide 3 km range resolution. The F-region mode, on the other hand, consists of a single 320 μs uncoded "long pulse" (LP) 48 km range resolution.

The high resolution "alternating code" (A16) scheme was implemented in part so that measured N_e profiles at E-region altitudes, where both the difference in electron and ion Hall mobility and the sum of electron and ion Pedersen mobility reach a maximum, are not degraded by smearing true ionospheric structure with a coarse 48 km sampling window. This "pulse smearing" effect, which typically *underestimates* Hall conductivity for highly structured arc-related N_e profiles, can also *overestimate* conductivity for quiet-time daylit profiles. Peak Hall conductivity for auroral arcs, in particular, is underestimated with LP samples by more than a factor of two.

Because A16 coding measures incoherent scatter from a 3 km range sample, its signal-to-noise ratio (SNR) is lower and usable altitude range is more restricted, when compared with the 48 km long-pulse sample. In practice, alternating-code measurements degrade rapidly above 200 km altitude. Typical up-B A16 measurements require at least 60 s of integration to yield usable estimates for electron and ion temperature from the IS fitter.

The LP mode, when used at altitudes above 200 km, provides an estimate for conductivity where typical F-region plasma structures have large intrinsic vertical scales and where Pedersen and Hall mobilities have large scale heights. Thus, F-region conductivity estimates from LP measurements are relatively insensitive to the effect of 48 km pulse smearing.

Herein we describe in detail a process to merge A16 and LP data streams in order to calculate height-resolved Pedersen and Hall conductivity. Sections 2 and 3 address background assumptions and algorithms for $N_e(z)$ merging and conductivity calculation. Section 4 provides a comparison of the resultant conductivity profiles and conductance calculation for a set of merged $N_e(z)$ profiles from experiments in which the ISR antenna was fixed up the local magnetic field line. These merged profiles represent two limiting cases of ionospheric production: 1) a nightside auroral arc, and 2) a quiet-time daylit ionosphere.

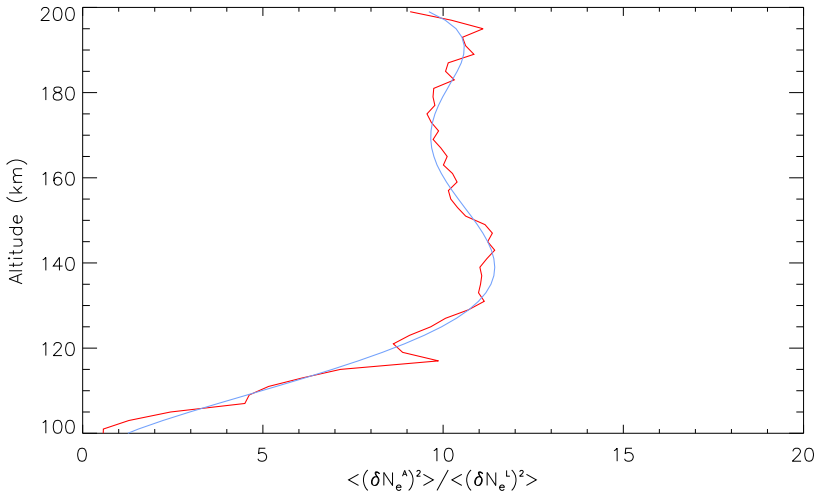

Figure 1: A16 Variance Normalization

Section 5 describes a method to calculate latitudinally-dependent conductivity from A16 and LP measurements acquired when the ISR antenna was scanning in elevation in the approximate plane of the magnetic meridian.

2. DATA MERGING

We have designed a merging process that uses N_e variance, provided by the ISR fitting program, to drive an altitude-dependent weighting that transitions smoothly from mostly A16 data at 90 km to mostly LP data at 200 km. As a first step, the N_e uncertainty yielded by the ISR fitter for these two data streams must be equalized. As indicated above, the A16 N_e measurement has a statistically lower SNR than the long-pulse measurements from the same altitude range. To first order, this lower SNR results in a higher relative uncertainty for A16 N_e measurements. Without some equalization of A16 N_e variance $\left(\delta N_e^A\right)^2$, LP data will be given too great a weighting in the E region. We emphasize that this equalization is only used in the weighting scheme.

In order to equalize variance for these two data streams, we calculate mean N_e variance, as a function of altitude, for both measurement modes with a large number of profiles. To this end, a Sondrestrom up-B ISR database was assembled with coordinated dual-mode measurements spanning a seven-year interval (18,000 profiles). The normalization factor shown in Figure 1, which indicates the ratio of mean N_e variance (A16) to mean N_e variance (LP), is used to reduce the raw A16 variance $\left(\delta N_e^A\right)^2$ of individual profiles prior to merging. The resultant equalized A16 variance $\left(\delta N_e^{A,eq}\right)^2$ has no statistical meaning beyond its use as a tool for merging N_e, δN_e, T_e, and T_i profiles from the A16 and LP data streams.

As a second step, the A16 and long-pulse data are sychronized and splined onto a uniform altitude grid at 2 km per element. Synchronization ensures that A16 and LP $N_e(z)$ measurements capture the temporal dynamics of the ionosphere in a coordinated fashion. The data are now set to merge in a manner that minimizes low-altitude pulse smearing.

N_e merging is accomplished with a weighting factor that minimizes the contributions from LP measurements at lower E-region altitudes. The merging takes the form

$$N_e = \frac{(\delta N_e^L)^2 N_e^A + f\left(\delta N_e^{A,eq}\right)^2 N_e^L}{(\delta N_e^L)^2 + f\left(\delta N_e^{A,eq}\right)^2}, \tag{1}$$

where the superscript L denotes LP measurements and f is the exponential weighting factor:

$$f = ae^{(z-z_0)/H_0}. \tag{2}$$

Coefficients a, z_0, and scale height H_0 have been selected so that $(\delta N_e^{A,eq})^2$ and $(\delta N_e^L)^2$ have equal weighting at 170 km and so that LP contributions are attenuated a factor of 400 at 90 km (relative to 200 km).

This merging approach is also applied to electron and ion temperature measurements as T_e and T_i are required in order to calculate electron and ion collision frequencies. The variance in merged electron density is given by substituting $(\delta N_e^A)^2$ and $(\delta N_e^L)^2$ for N_e^A and N_e^L in equation (1):

$$(\delta N_e)^2 = \frac{(\delta N_e^L)^2 (\delta N_e^A)^2 + f\left(\delta N_e^{A,eq}\right)^2 (\delta N_e^L)^2}{(\delta N_e^L)^2 + f\left(\delta N_e^{A,eq}\right)^2}. \tag{3}$$

Figures 2 and 3 provide examples of merged N_e profiles of active auroral and quiet daylit (solar zenith angle 74°) conditions, respectively. Error bars for the merged profiles are shown for reference. Both profiles have been integrated for 90 s.

The auroral profile shows how the coarse 48-km LP sampling attenuates the true peak of arc-related ionization at 115 km and adds an artifact below 105 km. The daytime profile, with a shape characteristic of an E-region ionosphere dominated by solar photoionization, shows less distortion from LP smearing.

A comparison of conductance determination as based on LP, A16, and merged up-B $N_e(z)$ profiles will be explored for both arc-related and daylit conditions in Section 4.

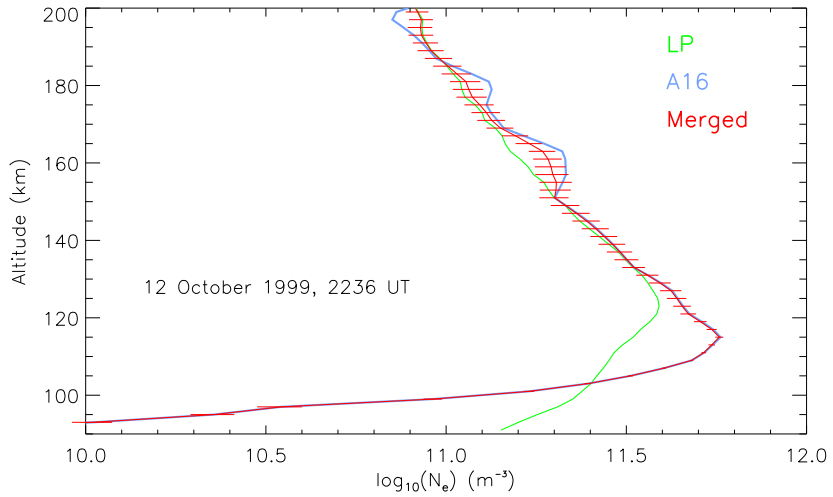

Figure 2: Merged $N_e(z)$ Profiles for an Auroral Arc

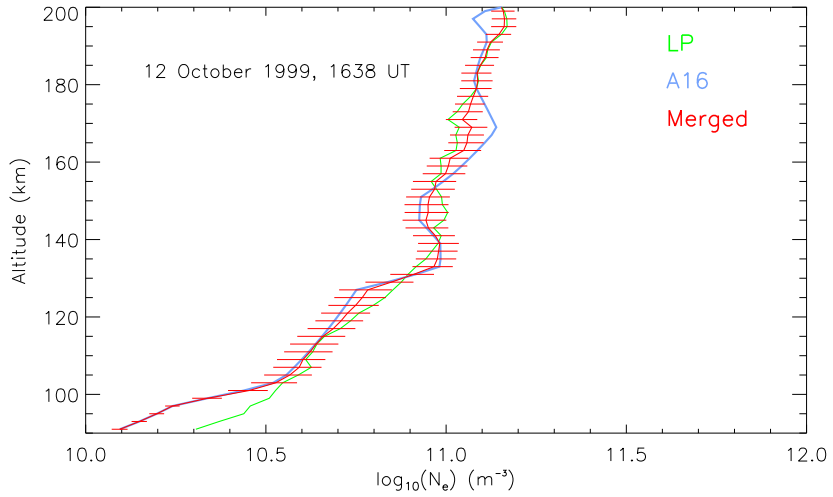

Figure 3: Merged $N_e(z)$ Profiles for Quiet Daytime Conditions

3. CONDUCTIVITY CALCULATION

Calculation of conductivity proceeds directly from a calculation of Pedersen and Hall mobilities as described by *Rishbeth and Garriott* [1969]. The calculation of mobility per unit charge (ratio of mean scattering time to mass) accounts for scattering contributions from both random thermal motions and ordered gyrorotation of ions and electrons in a background neutral atmosphere. Canonical forms for Pedersen mobility (k_1) and Hall mobility (k_2) are given:

$$k_1 = \frac{\nu/m}{\left(\nu^2 + \Omega^2\right)} \tag{4}$$

$$k_2 = \frac{\Omega/m}{\left(\nu^2 + \Omega^2\right)} \tag{5}$$

where ν is momentum transfer collision frequency of the ion or electron with background neutrals, m is mass of the ion or electron, and Ω is the ion or electron gyrofrequency (qB/m), where q is the ion or electron charge. Pedersen and Hall conductivity can now be given:

$$\sigma_P = N_e q^2 \left(k_{1e} + k_{1i}\right) \tag{6}$$

$$\sigma_H = N_e q^2 \left(k_{2e} - k_{2i}\right) \tag{7}$$

In determining Pedersen and Hall mobility, one can see that the gyrofrequency term Ω simply requires invoking a magnetic field model for B, such as the International Geomagnetic Reference Field [*IAGA*, 1985]. In order to determine all remaining ion and electron collision frequency terms in equations (4) and (5), additional empirical models and simplifying assumptions are required.

3.1 Electron Collision Frequency

Electron collision frequency comprises an electron-ion component (ν_{ei}) and an electron-neutral component (ν_{en}). The former can be calculated from the merged A16/LP $N_e(z)$ and $T_e(z)$ profiles using the formulation given by *Chapman* [1956]:

$$\nu_{ei} = N_e \times 10^{-6} \left(59 + 4.18\ log_{10}(T_e^3 N_e)\right) T_e^{-3/2}, \tag{8}$$

where N_e is expressed in MKS units and T_e in degrees Kelvin.

Calculating ν_{en} requires that we consider electron gas interaction with the neutral atmosphere. Specifically, [**O**], [$\mathbf{O_2}$], and [$\mathbf{N_2}$] altitude profiles are generated from the MSIS neutral atmosphere model [*Hedin*, 1987] for the date, time, and geophysical state associated with the profile in question. The total electron-neutral collision frequency can be cast to include contributions from [**O**], [$\mathbf{O_2}$], and [$\mathbf{N_2}$],

$$\nu_{en} \;=\; \nu_{e_O} \;+\; \nu_{e_{O_2}} \;+\; \nu_{e_{N_2}}, \tag{9}$$

where individual components are given by *Schunk and Nagy* [1978]:

$$\nu_{e_O} \;=\; 8.9 \times 10^{-17}\,[\mathbf{O}]\,\left(\,1 + 5.7 \times 10^{-4}\,T_e\,\right)\,\sqrt{T_e} \tag{10}$$

$$\nu_{e_{O_2}} \;=\; 1.82 \times 10^{-16}\,[\mathbf{O_2}]\,\left(\,1 + 3.6 \times 10^{-2}\sqrt{T_e}\,\right)\,\sqrt{T_e} \tag{11}$$

$$\nu_{e_{N_2}} \;=\; 2.33 \times 10^{-17}\,[\mathbf{N_2}]\,\left(\,1 + 1.21 \times 10^{-4}\,T_e\,\right)\,T_e, \tag{12}$$

and MKS units are assumed.

3.2 Ion Collision Frequency

We choose to follow the common practice of ignoring the ion-electron contribution (ν_{ie}) to the total ion collision frequency. In order to evaluate ν_{in} we will consider all nine combinations of an O^+, O_2^+, NO^+ ionosphere interacting with an O, O_2, and N_2 neutral atmosphere.

Our approach will be to calculate terms involved with a single ionic species, that is,

$$\nu_{_{O^+}} \;=\; \nu_{_{O^+O}} \;+\; \nu_{_{O^+O_2}} \;+\; \nu_{_{O^+N_2}}, \tag{13}$$

$$\nu_{_{O_2^+}} \;=\; \nu_{_{O_2^+O}} \;+\; \nu_{_{O_2^+O_2}} \;+\; \nu_{_{O_2^+N_2}}, \tag{14}$$

$$\nu_{_{NO^+}} \;=\; \nu_{_{NO^+O}} \;+\; \nu_{_{NO^+O_2}} \;+\; \nu_{_{NO^+N_2}}, \tag{15}$$

and then form a composite collision frequency weighted by the fractional abundance of O^+, O_2^+, and NO^+:

$$\nu_{in} \;=\; q_{_{O^+}}\;\nu_{_{O^+}} \;+\; q_{_{O_2^+}}\;\nu_{_{O_2^+}} \;+\; q_{_{NO^+}}\;\nu_{_{NO^+}}. \tag{16}$$

This plan necessarily requires that we use a model for the altitude transition from molecular to atomic ions. The model used presently is the formulation of *Evans and Oliver* [1972] and *Oliver* [1975] for the fractional abundance of $[\mathbf{O}^+]$ relative to total plasma density N_e:

$$q_{O^+} = \frac{2}{1 + \sqrt{1 + 8 \exp\left[-(z - z_{50})/H\right]}}, \tag{17}$$

where z_{50} is the transition-altitude where a 50–50% mix of molecular and atomic ions exists. H is the transition scale height. The *Oliver* [1975] model found H to be a strong function of $[\mathbf{O}_2]$ and $[\mathbf{N}_2]$ scale heights that can be expressed in general terms as

$$H = H_\infty \frac{\left[T_\infty - (T_\infty - T_{120})\exp\Big(-a(z - 120)\Big)\right]}{t_\infty}, \tag{18}$$

where H_∞ is a reference scale height at the exobase, T_∞ is exospheric temperature, and T_{120} is the neutral temperature at 120 km.

The temperature shaping coefficient a was set to 0.01 km^{-1} and H_∞ set to 20 km in equation (18) in order to best agree with the high-latitude ISR ion composition profiles reported by *Kelly* [1980]. In that study, values of z_{50} varied from 170 to over 200 km depending on the state of auroral precipitation and Joule heating. A value of 185 km, representative of an ionosphere with some auroral activity, has been adopted in the present calculations. Values of T_∞ are supplied from the MSIS model.

Once q_{O^+} has been determined, one must determine how to partition the abundance of molecular ions between O_2^+ and NO^+. For the present calculation we assume a 1:3 mix of O_2^+ and NO^+ so that

$$q_{O_2^+} = 0.25\ (1 - q_{O^+}), \tag{19}$$

$$q_{NO^+} = 0.75\ (1 - q_{O^+}), \tag{20}$$

with aggregate ion mass m_i given by

$$m_i = m_P\ (16\ q_{O^+} + 32\ q_{O_2^+} + 30\ q_{NO^+}), \tag{21}$$

where m_P is the mass of a proton. We now consider the nine individual ion-neutral collision terms described in equations (13) through (15).

Debate over the most appropriate form for the resonant atomic oxygen ion-neutral collision frequency has diminished considerably following the recommendation of *Salah* [1993] that a scaling factor be used to bring prior theoretical and laboratory expressions into agreement with actual thermospheric measurements. For the present calculation, we use the expression derived by *Schunk and Walker* [1970] modified with the 1.7 "Burnside Factor" [*Salah*, 1993]:

$$\nu_{O^+O} = 1.7 \times 3.42 \times 10^{-17} \, [\mathbf{O}] \, \sqrt{T_m} \left[1.08 - .139 \, log_{10}(T_m) + 4.51 \times 10^{-3} \, (log_{10}(T_m))^2\right], \quad (22)$$

where T_m is the average of ion and neutral temperature.

Expressions for the molecular oxygen resonant charge exchange collision frequency used in the present calculation are given by *Banks* [1966]:

$$\nu_{O_2^+O_2} = 2.4 \times 10^{-19} \, [\mathbf{O_2}] \, \sqrt{T_m} \left[10.4 - 0.76 \, log_{10}(T_m)\right]^2 \quad T_m > 800^\circ K \quad (23a)$$

$$\nu_{O_2^+O_2} = 4.08 \times 10^{-16} \, [\mathbf{O_2}] \quad T_m < 800^\circ K \quad (23b)$$

Expressions used in the present calculation for the remaining seven non-resonant collision frequencies have been formulated by *Schunk and Nagy* [1980]:

$$\nu_{O^+O_2} = 6.64 \times 10^{-16} \, [\mathbf{O_2}] \quad (24)$$

$$\nu_{O^+N_2} = 6.82 \times 10^{-16} \, [\mathbf{N_2}] \quad (25)$$

$$\nu_{O_2^+O} = 2.31 \times 10^{-16} \, [\mathbf{O}] \quad (26)$$

$$\nu_{O_2^+N_2} = 4.13 \times 10^{-16} \, [\mathbf{N_2}] \quad (27)$$

$$\nu_{NO^+O} = 2.44 \times 10^{-16} \, [\mathbf{O}] \quad (28)$$

$$\nu_{NO^+O_2} = 4.27 \times 10^{-16} \, [\mathbf{O_2}] \quad (29)$$

$$\nu_{NO^+N_2} = 4.34 \times 10^{-16} \, [\mathbf{N_2}]. \quad (30)$$

These expressions are evaluated based on MSIS neutral atmosphere model runs for the date, time, and geophysical conditions specified for merged N_e, T_e, and T_i profiles. Conductivity calculation now proceeds by evaluating the mobilities in equations (4) and (5) and substituting the result into equations (6) and (7). Height-integrated conductivity, or conductance, is formed by integrating σ_P and σ_H over an altitude range from 90 to 500 km.

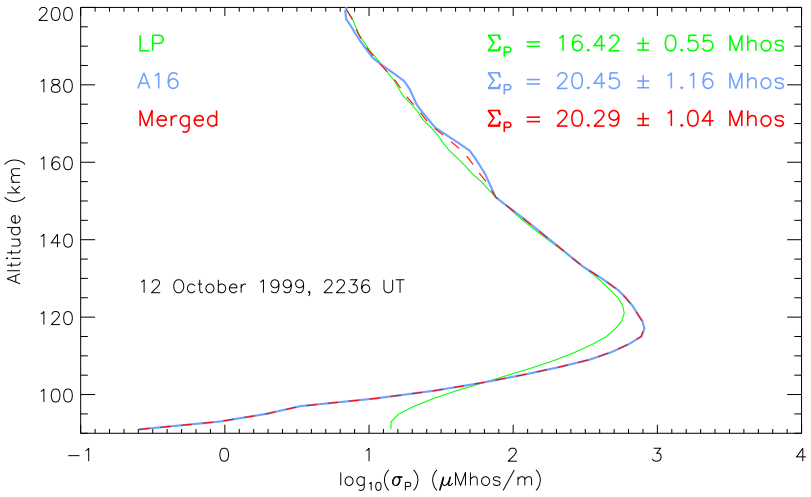

Figure 4: Merged $\sigma_P(z)$ Profiles for an Auroral Arc

3.3 Calculation of Conductivity Uncertainty

Because conductivity is linear with $N_e(z)$ as indicated in equations (6) and (7), we conclude that the conductivity uncertainty should then be proportional to δN_e. In order to calculate $\delta\sigma_P$ and $\delta\sigma_H$, we simply take the square-root of the merged N_e variance, given in equation (3), and treat it as a pertubation N_e to the calculation of conductivity described in equations (4) through (30) above. All other inputs required for conductivity, that is, the MSIS and IGRF models, the *Oliver* [1975] model, and the nominal $T_e(z)$ and $T_i(z)$ profiles, remain unchanged.

4. COMPARISON OF LP AND MERGED CONDUCTANCE ESTIMATES

The dashed red curve in Figure 4 shows the resultant Pedersen conductivity profile for the arc-related merged N_e profile shown in Figure 2. Green and blue profiles, calculated from the unmerged LP and A16 measurements, are provided for reference. This plot shows how the 320-μs long pulse (green profile) raises the Pedersen conductivity peak altitude, reduces the Pedersen conductivity peak by 20%, and widens the profile significantly below 105 km. Upon height integration, one sees that attenuation of conductivity at the peak dominates over addition of the low-altitude widening to yield an estimate for Σ_P that is 20% too low.

Corresponding arc-related Hall conductivity and conductance are given in Figure 5. In this case, Σ_H is underestimated by approximately 10%. However, it is the cancelling of two diverse effects that make the conductance difference small.

Figures 6 and 7 summarize Pedersen and Hall conductivity and conductance calculation for

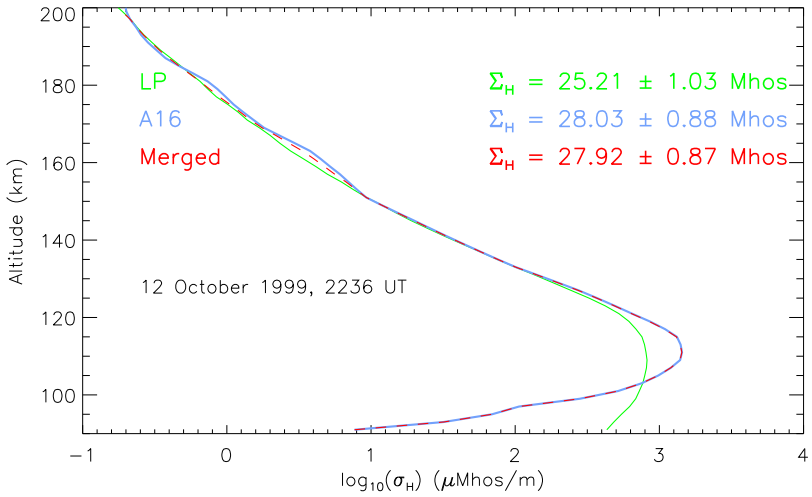

Figure 5: Merged $\sigma_H(z)$ Profiles for an Auroral Arc

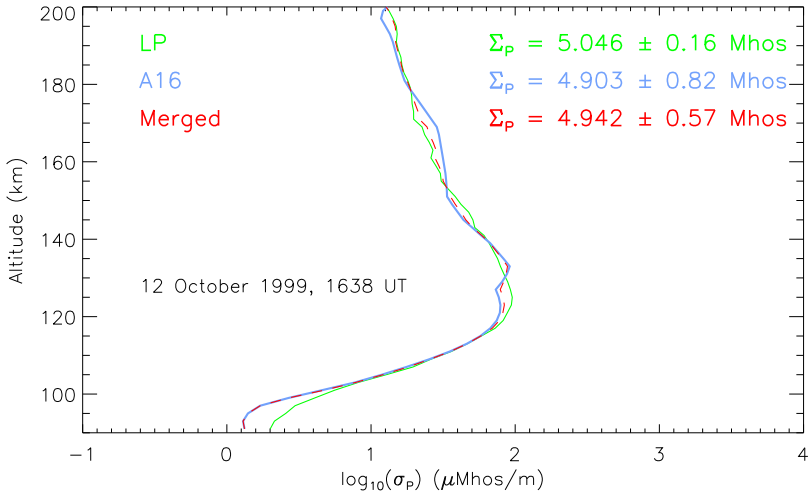

Figure 6: Merged $\sigma_P(z)$ Profiles for Quiet Daytime Conditions

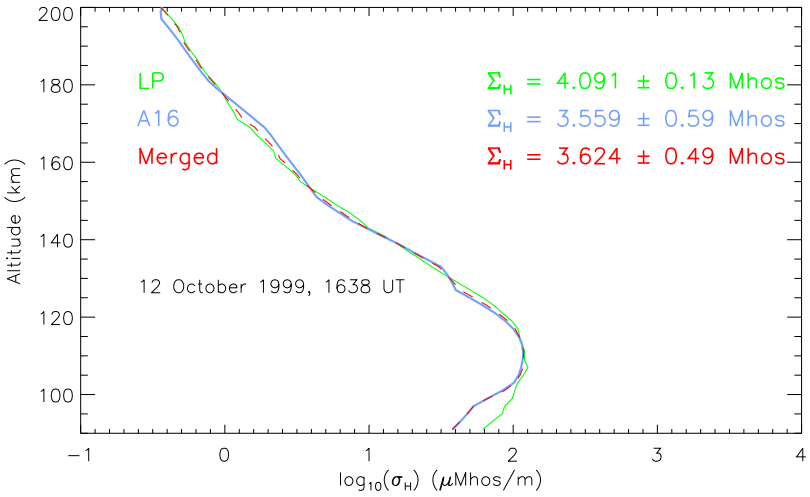

Figure 7: Merged $\sigma_H(z)$ Profiles for Quiet Daytime Conditions

the quiet sunlit $N_e(z)$ profile previously presented in Figure 3. With no arc-related peak in ionization, the dominant effect of LP pulse smearing is simply the addition of conductivity below 105 km. Σ_P and Σ_H are consequently overestimated by 2% and 12%, respectively.

5. CONDUCTIVITY FROM LP AND A16 SCAN DATA

ISR dwell experiments are essential in characterizing up-B plasma parameters of auroral structure. For dynamic events such as a substorm expansion or the transit of polar patches, however, ionospheric features will rarely linger above the local field line. For such periods, and for studies of magnetospheric boundaries in general, the ISR is more effectively employed by scanning across many lines of force in the plane of the magnetic meridian. Such a mode captures plasma structure across a large latitude-altitude field of view and describes the evolution of such structure on a typical time scale of minutes.

The first ever scan experiments were conceived when the Sondrestrom ISR was located in the auroral zone at Chatanika, Alaska [*Vondrak and Baron*, 1976]. This early work underscored the ability of elevation scans to describe the latitudinal variation of field-aligned plasma structure and of the energy spectra of the precipitating electrons. Later scan experiments were coordinated with *in-situ* sounding rockets to measure electrodynamic and plasma parameters associated with stable boundary arcs [*Niciewjewski et al.*, 1988] and with sun-aligned polar cap arcs [*Berg et al.*, 1993].

Herein, we describe how to derive conductivity from dual LP and A16 scan experiments. The essential feature of an ISR scan, that is, its wide latitudinal coverage over a timescale of minutes, necessarily requires thoughtful tradeoffs between spatial and temporal coverage

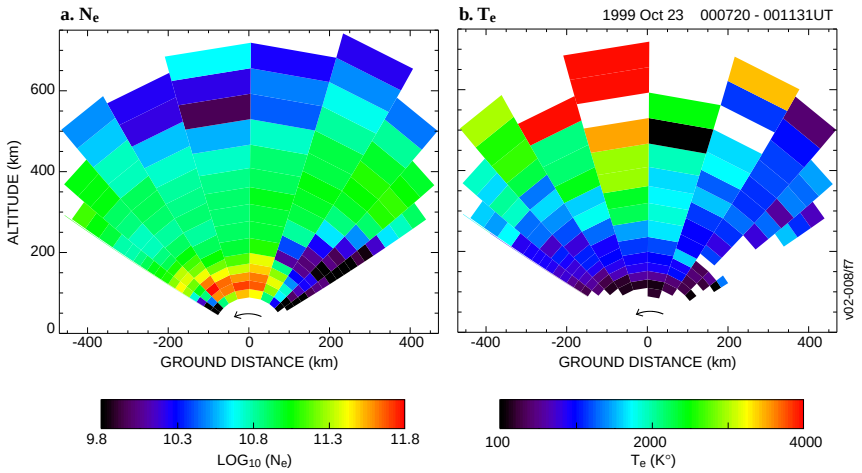

Figure 8: N_e and T_e During a Substorm Expansion Event

as well as a scheme for deriving conductivity from noise-dominated N_e profiles. In the latter case, the ISR fitter will mostly fail to provide usable estimates of T_e and T_i for both LP and A16 data streams.

In the sections that follow, we describe sampling and mapping issues pertaining to ISR elevation scans, motivate the use of model-temperature-corrected 'Raw N_e' for the LP data stream, discuss inclusion of A16 Raw N_e so as to avoid the pulse-smearing effects, and summarize merging and conductivity results for a dynamic substorm expansion event.

5.1 Temporal and Spatial Resolution

Full ISR 'elscans' typically span 120° of elevation angle in order to cover a latitude range of 10° and 3° in the *F*- and *E*-regions, respectively. Scan periods of 180 to 300 s are typically used to measure large scale auroral boundary and polar cap patch motion. Each scan is segmented into discrete angular samples, or 'records', which correspond to a fixed interval of time Δt over which range-resolved IS spectra are integrated. Figure 8 summarizes LP N_e and T_e acquired during a scan of a dynamic auroral arc. In this figure, ten records are sampled in approximately 4 minutes. The slew rate of the antenna has been adjusted so that each 25-s record covers a fixed horizontal ground distance – a so-called 'variable scan rate' or VSR scan.

Although such 4 min elevation scans will smooth out detailed structure from dynamic aurora, faster antenna motion presents fundamental sampling problems. In practice, elevation scan samples acquired by the Sondrestrom ISR with Δt less than ~10 s are insufficiently integrated to yield high quality IS spectra. Recall that the up-B $N_e(z)$ profiles shown in Figures 2 and 3 were derived from 90 s integrations. In order for IS

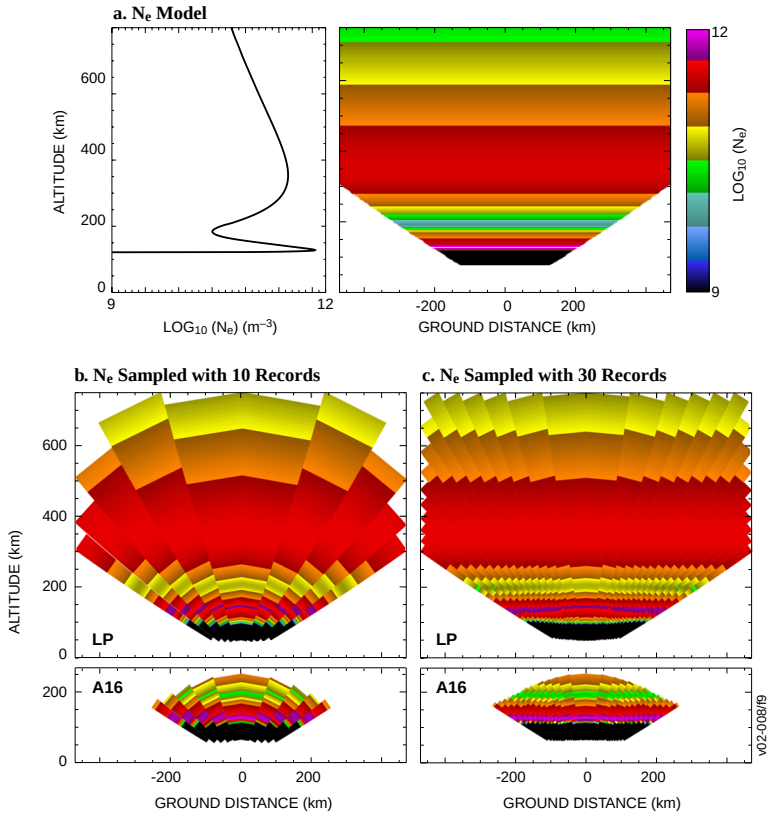

Figure 9: Structural Effects from Elevation Scan Sampling

spectra from the scan in Figure 8 to have the same SNR as for the up-B profiles, the full scan period would be 15 minutes – a time scale clearly unusable for studies of typical auroral phenomena. Thus, the elevation scan rate is selected so that ΔT is greater than the minimum time required to acquire 'usable' IS spectra and less than the maximum 'smearing' time acceptable for dynamic ionospheric structure. Calculation of conductivity from short noise-dominated scan records will force us to use N_e estimates based on T_e and T_i values from a model, rather than the ISR fitter.

Calculation of conductivity from elevation scans also requires placing the data into bins of altitude and latitude – a process necessarily dependent on the granularity of spatial samples. For scans, the measured volume is a sector bounded by two values of range and two values of elevation angle θ. The measured line-of-sight electron density $N_e(r, \theta_0)$, at a range resolution given by the transit time of the pulse traveling at the speed of light ($r_p = c\tau/2$) and over an angular range from θ_1 to θ_2 is defined as

$$N_e(r, \theta_0) = \int_{\theta_1}^{\theta_2} \frac{r^2}{r_p} \int_{-r_p/2}^{r_p/2} \frac{N_e^0(r)}{r^2}\, dr\, d\theta, \tag{31}$$

where $N_e^0(r)$ is the intrinsic electron density along a radial from the IS radar, and r_p is 48 km for LP mode and 3 km for A16 mode. For LP measurements, raw $N_e(r)$ (Section 5.3) is calculated for 14 μs subsamples of the 320 μs pulse yielding 2.1 km *correlated* samples.

In order to intuitively understand the effect of range and angular sampling, we have created a model array of N_e with known vertical morphology and completely uniform horizontal structure. Figure 9*a* shows the modeled $N_e(z)$ profile and Figure 9*b* places it on a horizon coordinate grid assumed to be the plane of the local magnetic meridian. The N_e altitude structure has been modeled as produced from a 100 keV monoenergetic electron beam (number flux of 10^8 cm^{-2} s^{-1}) with an added Chapmanlike *F*-layer at 300 km. The bottomside thickness of the *E*-region ionization is only 4 km and was chosen to help minimize systematic errors in the end-to-end calculation of conductance.

Panel (c) shows how the model N_e array looks after having been sampled with the LP mode according to equation (31) with the same 10-record angular scheme as used in the scan of Figure 8. Panel (d) shows samples from a notional 30-record scan. In each panel, LP samples are shown at the top and A16 samples (up to ~200 km range) are shown on the bottom. Most notable in panel (c), one can recognize the introduction of horizontal 'corrugation' structure as an artifact of angular sampling. Range smoothing, which results in the failure of LP samples to reproduce the green 'valley' of ionization at 200 km (upper portion of Panels (c) and (d)), also significantly attenuates and shifts the peak of the low-altitude *E*-region structure. The impact of these geometrical effects on Pedersen and Hall conductance estimates will be summarized later in Section 5.5.

5.2 Magnetic Mapping of ISR Scan Data

A basic presumption in high-latitude ionospheric physics is that auroral structure should be oriented with the geomagnetic field. A common practice, thus, is to map scanned plasma parameters from the fundemental measurement basis of elevation angle and range onto a grid defined by geomagnetic latitude and altitude. This mapping attempts to preserve the relationship between high- and low-altitude plasma measurements causally related to magnetospheric processes. For conductivity studies, the range of geomagnetic latitudes covered is limited to a 3^o span over which scanned field lines thread both *E*- and *F*-region altitudes.

Figure 10*a* shows how records from a 10-record elevation scan overlap with contours of constant geomagnetic latitude. The specific geomagnetic lines shown are from the PACE model [*Baker and Wing*, 1989], which is a spherical coordinate expansion of the International Geomagnetic Reference Field (IGRF) [*IAGA* 1985]. Both IGRF and PACE models calculate a time-dependent B-field by means of annually updated coefficients which are based on the observed secular evolution of the Earth's magnetic field.

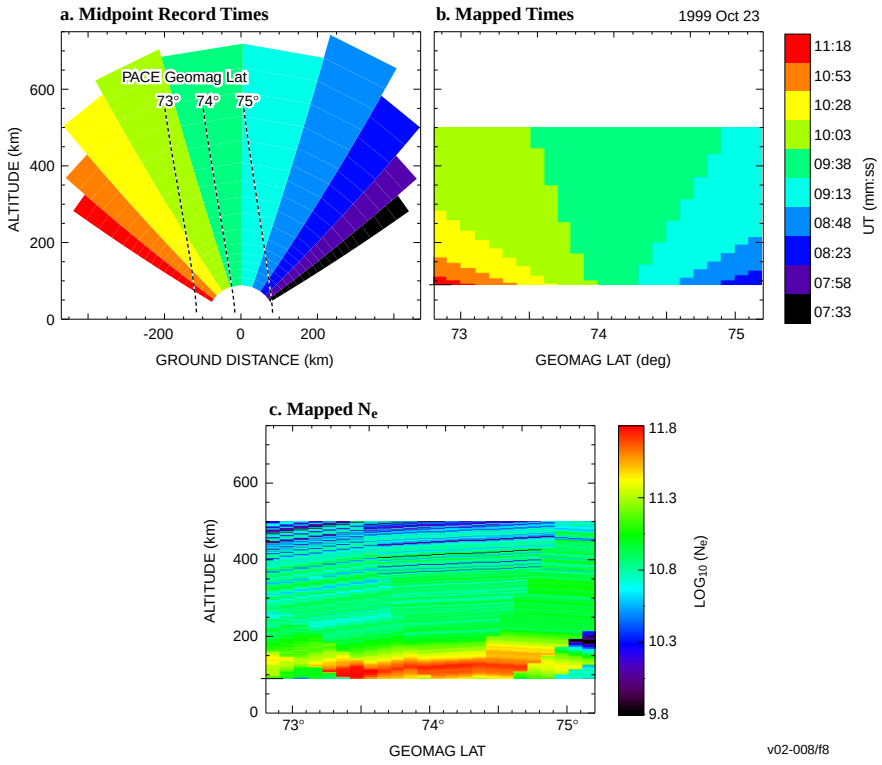

Figure 10: Mapping Scans from Horizon to Geomagnetic Coordinates

Panel (a) color-codes the time associated with each individual record's integration as the antenna sweeps from north to south in 250 s. Panel (b) shows how this scan time maps via the PACE geomagnetic model to a plane defined by Λ and an altitude range of 100 to 500 km. Note how the first 50 s of scan time (associated with records that cut across many field lines to the north) do not map to the geomagnetic plane. This result merely emphasizes our requirement that, for conductivity studies, we need to fill both *E*- and *F*-region measurements in a given geomagnetic latitude bin. Panel (b) also shows how data along an individual latitude is contributed from as many as four sequential records. Panel (c) shows the raw electron density data (see Section 5.3) corresponding to the scan in Figure 8*a* as mapped to the geomagnetic plane. Note that mapped $N_e(z)$ profiles show a high degree of correlation, especially in Λ bins from 73.5^o to 75.5^o. Such correlation indicates that N_e from a 10-record VSR scan is highly oversampled at 0.1^o resolution in Λ. A more appropriate Λ bin for this scan is 0.3^o

We now examine the use of temperature-corrected LP raw N_e and uncorrected A16 raw N_e as a way to significantly enhance the accuracy of our conductance measurements.

5.3 The use of Raw $N_e(z)$ in Conductance Calculation

The short integation time of ISR scan records, relative to dwell Δt's, yield estimates of plasma N_e, T_e, and T_i from the IS fitter which are predictably noisey. For A16 scan data, the IS fits are so unreliable that we choose to include only the A16 raw N_e data stream in our conductivity calculation.

For the LP data stream, one needs to make best use of available raw N_e estimates and whatever sparse T_e and T_i measurements are available. Herein, we review the definition of raw N_e in the context of the radar equation, and describe a method to 'temperature correct' the raw LP N_e with a splined version of T_e and T_i.

Any radar system can be described by the classical radar equation, which relates power supplied by the transmitter, P_t, to the scattered power available at the receiver, P_r. For monostatic continuous wave operation this relation becomes, after *Ridenour* [1947]:

$$P_r \;=\; P_t \left(\frac{GA}{16\pi^2 r^4}\right) \sigma, \tag{32}$$

where G is the effective on-axis antenna gain (relative to isotropic directivity), A is the antenna receiving area, r is the range to the center of the scattering volume, and σ is scattering cross section, in units of m^2.

For a beam-filling target, such as an ionospheric plasma, the cross section, σ, is a function of the volume and number density of scatterers. Because scattering volume is proportional to the square of range, the severe r^{-4} attenuation of power described by Equation 32 is reduced to r^{-2} for an ionospheric IS radar. Ionospheric radars must also recover

range-resolved measurements and so must pulse the transmitter.

Evans [1969] determined a more applicable form for the radar equation by integrating the gain of an assumed parabolic reflector over all solid angles to yield

$$P_r \;=\; P_t \left(\frac{0.76\; Lc\tau A}{16\pi r^{\,2}}\right) N_e\sigma, \tag{33}$$

where L represents ohmic insertion losses to and from the antenna, c is the velocity of light, τ is the transmitted pulse period, and σ is the incoherent backscatter cross section. This exercise assumes that N_e varies little over the sampled pulse range ($c\tau/2$) – an assumption that tends to break down when the 48 km LP mode is used to probe *E*-region structure (see low altitude portion of Figure 8*b*). The salient feature of this relationship is that power returned to the receiver from an ISR pulse is proportional to the volume density of the ionospheric plasma and its scattering cross section.

This cross section, σ, a frequency-dependent quantity that results from the interaction of an incident electromagnetic wave with a volume of geophysical plasma, effectively describes the collective behavior of thermal fluctuations in the plasma's refractive index. σ has two components: a so-called 'ion line' which is dependent on the ISR wavelength (λ_R), ion-neutral collision frequency, bulk plasma drift, plasma density, ion and electron temperature, and ion composition, and an electron 'plasma line' which, under the right conditions, can be used to very accurately gauge absolute N_e.

A typical IS fitting algorithm makes initial assumptions that ion and electron components of the plasma are individually in thermodynamic equilibrium and that the ion composition is known, and then determines from the ion line spectra optimal estimates for N_e, T_e, T_i, and ion drift.

A functional form for the magnitude of the ion component of σ was derived by *Buneman* [1962] with the assumption that electrons and ions had individual Maxwellian velocity distributions described by temperatures T_e and T_i, respectively. This expression, generally valid for T_e/T_i less than 4, takes the form

$$\sigma \;=\; \left(\frac{\sigma_e}{(1\;+\;\alpha^2)\;(1\;+\;T_e/T_i\;+\;\alpha^2)}\right), \tag{34}$$

where σ_e is the Thompson backscatter cross section of a free electron, α is the Debye correction factor

$$\alpha \;=\; 4\pi\lambda_D/\lambda_R, \tag{35}$$

λ_D is the electron Debye length

$$\lambda_D \;=\; \left(\epsilon_0 kT_e/4\pi N e^{\,2}\right)^{1/2}, \tag{36}$$

k is Boltzman's constant, and ϵ_0 is the permittivity of free space.

We can now substitute equation (34) into equation (32), absorb σ_e into the other constants, and solve for electron density in the manner given by *Baron* [1977]

$$N_e \;=\; (A)\left(\frac{1}{P_t\tau}\right)(r^2 P_r)\left(\frac{(1\;+\;\alpha^2\;+\;T_e/T_i)(1\;+\;\alpha^2)}{2}\right), \tag{37}$$

where A is a lumped system constant. Operationally, constant A is determined during periods when the electron plasma line can be measured *Evans* [1969]. For the Sondrestrom IS radar, the system constant has most recently been measured at 3.548×10^{19}s m^{-5} [*Heinselman*, 1999].

Equation (37) is thus separated into four brackets corresponding to (1) constants, (2) variables that are usually fixed during a particular experiment, (3) variables which are measured, and (4) parameters determined from spectral analysis of the ion line component of σ.

'Raw N_e' is a special form of simple raw power, wherein equation (37) is evaluated with the fourth bracket set to 1. This assumption, that T_e/T_i is unity and α is zero, allows raw N_e to be derived in the absence of ion line spectral analysis. Because spectral analysis is typically performed post experiment, raw N_e has proved to be a popular real time diagnostic for experiments which require rapid assessment of ionospheric plasma structure, such as sounding rocket campaigns. For the short integration time noise-dominated measurements acquired during scans, raw N_e is often the only parameter available from the ISR.

Brekke and Moen [1993] point out that because T_e is usually greater than T_i, especially in the F-region, the fourth bracket of equation (37) will be greater than 1 and raw N_e will always be an underestimate of real N_e. When using raw N_e to calculate conductivity, they report attenuated peaks on the order of 10 to 30 percent. We should thus try to temperature correct the LP Raw N_e in order to provide a more accurate gauge of conductance. As mentioned at the beginning of this section, A16 scan data are thouroughly noise dominated, eliminating the possibility for the temperature correction of A16 raw N_e.

5.4 Temperature Correction of LP Raw $N_e(z)$

Spectral analysis from LP scan data yields T_e and T_i estimates with (at best) 48-km range resolution. At altitudes well above the peak of the F-layer, the recovered SNR attenuates considerably resulting in predictably sparse profiles of electron and ion temperature. As mentioned previously, the 320 μs LP is oversampled at 14 μs resulting in raw $N_e(z)$ samples with apparent 2.1 km range resolution. Rather than representing independent samples, these 2.1 km measurements are subsamples of a convolution of the 48-km pulse with the intrinsic structure of the ionospheric plasma. In the absence of sharp gradients in $N_e(z)$, these raw samples provide a clear picture of vertical N_e morphology. For the purpose of calculating conductance in the F-region, 2.1 km *correlated* N_e samples also allow

estimates of $\sigma_P(z)$ and $\sigma_H(z)$ to be made on a grid better suited for vertical integration than the irregularly spaced ranges corresponding to T_e and T_i estimates.

We therefore choose to spline the coarsely sampled T_e and T_i profiles onto the 2.1 km resolution of the raw N_e data subsequent to magnetic mapping. In order to constrain the splining algorithm to physically reasonable temperatures beyond the range of ISR measurements, low- and high-altitude tie points must be established. The MSIS neutral atmospheric model [*Hedin*, 1987] is used at low altitudes (where one expects $T_e = T_i = T_n$), and the IRI ionospheric model is used at 800 km. Subsequent to splining, temperature-correction procedes by evaluating the fourth bracket of equation (37). Because α scales as $N_e^{-1/2}$, equation (37) is non-linear in N_e, and a solution for temperature-corrected N_e is thus determined by a simple numerical iteration.

As noted in Section 4, pulse smearing effects of the temperature-corrected LP N_e can be as great as -50% for peak Pedersen conductivity for auroral arc conditions. Therefore, in order to mitigate the effects of LP mode pulse smearing on conductivity calculation, we will merge temperature-corrected LP N_e with available raw A16 N_e for scans. This merging procedes as described in Section 2.

5.5 Effect of Finite Angular and Range Sampling on Σ Estimates

In order to assess the end-to-end sensitivity of our scan conductance method to spatial sampling effects, we return again to the model ionospheric profile presented in Figure 9*a*. The conductance calculated from this profile is dominated by the thin 4-km-thick *E*-region peak at 130 km. Distortions in the shape of the N_e model due to angular integration, pulse smearing, or magnetic mapping, summarized graphically in Figure 9*b* through Figure 9*d*, will now propagate through the merging and conductance calculation described in Sections 2 and 3.

Figure 11 summarizes Pedersen and Hall conductance deviations for various sampling schemes. The modeled Σ_P and Σ_H for the profile of Figure 9*a* are 17.6 and 7.06 Mhos, respectively. Each plot shows how the conductance varies across the 3° range of geomagnetic latitude centered on the location of the Sondrestrom ISR. Because the model has been designed to be uniform across all latitudes, any deviations from modeled values of Σ_P and Σ_H must be due to quantization and magnetic mapping effects.

The color-coded legend from black to red indicates a progression of increasing precision in both range and angular resolution. The black and blue lines correspond to LP mode sampling (that is 48 km pulse smearing) at 10 and 30 records, respectfully. The green and orange lines indicate the effect of adding the raw N_e from the A16 mode to the LP input data streams. The red line indicates estimated conductance for a sampling scheme with no pulse smearing (NPS) and 1° (120 record) angular resolution. The Λ bins have been set to 0.1^o for the 30- and 120- record samples and set to 0.3^o for the 10-record samples.

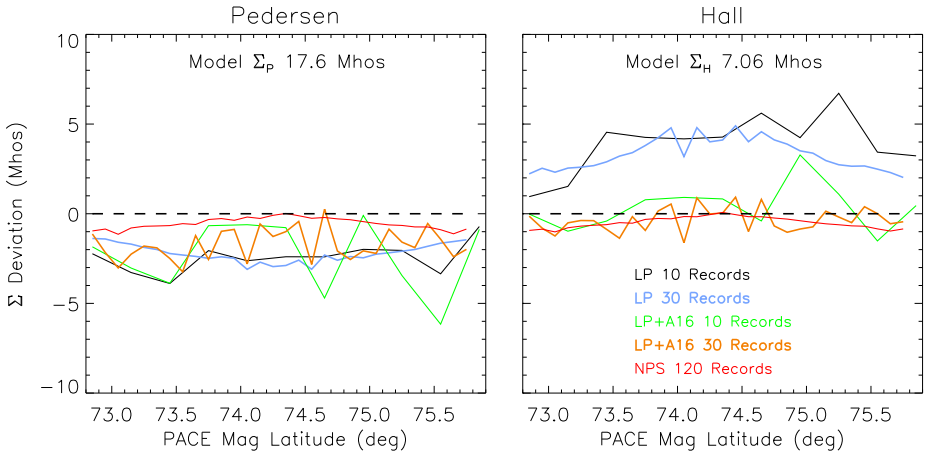

Figure 11: Σ Deviation from Model with 100 keV Beam ($\Delta z = 4$ km)

The 1-Mho deviations of the NPS 120-record sample from the model respresents the limiting precision of sampling due to the finite 1-km granluarity of our altitude grid. In general, this figure shows that spatial distortions serve to underestimate Σ_P and overestimate Σ_H for these auroral arc conditions by significant amounts. In all cases, inclusion of A16 raw N_e helps bring the estimate closer to the model. There is a suggestion from this plot that 10-record scan samples to the north, which intersect more lines of magnetic force, have greater error relative to the model.

References

Banks, P. M., Collision frequencies and energy transfer, ions., *Planet. Pace Sci., 14*, 1105, 1966.

Baron, M. J., The Chatanika radar system, in *Radar Probing of Auroral Plasma,* edited by A. Brekke, pp 103 - 142, Universitetsforlaget, Oslo, 1977.

Brekke, A. and J. Moen, Observations of high latitude ionospheric conductances - A review, *J. Atmos. and Terr. Phys., 55*, 1493, 1993.

Buneman, O., Scattering of radiation by the fluctuations in a nonequilibrium plasma, *J. Geophys. Res., 67*, 2050, 1962.

Chapman, S., The electrical conductivity of the ionosphere: A review, *Nuovo Cimento, 4*(10), suppl. 4, 1385, 1956.

Evans, J. V. and W. L. Oliver, The study of *E*-region ion concentration and composition by incoherent scatter radar, *Radio Sci., 7*, 103, 1972.

Heinselman, C. J., *Auroral Effects on Meteoric Metals in the Upper Atmosphere*, Ph.D. Dissertation, Stanford University, Palo Alto, 1999.

Hedin, A. E., MSIS-86 thermospheric model, *J. Geophys. Res., 92*, 4649, 1987.

International Association of Geomagnetism and Aeronomy (Division I Working Group), International geomagnetic reference field: Revision 1985, *J. Geomagn. Geoelectr., 37*, 1157, 1985.

Kelly, J. D., *Radar Measurements of Temperatures and Ionic Composition in the High-Latitude Ionosphere*, Ph.D. Dissertation, University of Alaska, Fairbanks, 1980.

Kelly, J. D., C. J. Heinselman, J. F. Vickrey, and R. R. Vondrak, The Sondrestrom radar and accompanying ground-based instrumentation, *Space Sci. Rev., Vol 71*, 797, 1995.

Moen, J. and A. Brekke, The solar flux influence on quiet-time auroral ionospheric conductances, *Geophys. Res. Lett., 20*, 971, 1993.

Oliver, W. L., Models of *F1*-region composition variations, *J. Atmos. Terr. Phys., 37*, 1065, 1975.

Ridenour, L. N., *Radar System Engineering*, Vol. 1, Radiation Laboratoty Series, McGraw-Hill, New York, 1947.

Rishbeth, H. R. and O. K. Garriott, *Introduction to Ionospheric Physics*, Academic Press, New York and London, 1969.

Salah, J. E., Interim standard for the ion-neutral atomic oxygen collision frequency, *Geophys. Res. Lett., 20*, 1543, 1993.

Schunk, R. W. and A. F. Nagy, Electron temperatures in the F region of the ionosphere: theory and observations, *Rev. Geophys. and Space Phys., 16*, 355, 1978.

Schunk, R. W. and J. C. G. Walker, Thermal diffusion in the *F2* region of the ionosphere, *Planet. Space Sci., 20*, 1319, 1970.

Vondrak, R. R. and M. J. Baron, Radar measurements of the latitudinal variation of auroral ionization, *Radio Sci., 11*, 939, 1976.